RSAR: Restricted State Angle Resolver and Rotated SAR Benchmark

Supplementary Material

A. Proof of Three-dimensional Mapping

In Sec. 3.1, we introduce constraints for three-dimensional mapping and present Eqn. (4). We will provide the detailed deduction and proof in this section.

We assume that the encoded values follow the same distribution across each dimension, implying that the absolute values of the weights of each dimension are equal. To simplify, we further assume that all dimensions have identical weights. Based on this assumption, the following formula can be derived:

$$m_1 + m_2 + m_3 = 0. \tag{9}$$

This equation describes the two-dimensional plane in which the mapping data resides. The normal vector of the plane can be expressed as $\boldsymbol{w} = [1, 1, 1]^T$.

One-dimensional values are mapped into a three-dimensional unit space (*i.e.*, each dimension has a value range of $[-1, 1]$) to form a circular curve. Given this condition and the plane defined in Eqn. (9), we can derive that the distance from any encoded values to the origin is equal to $\frac{3}{2}$. Thus, we derive the following formula:

$$m_1^2 + m_2^2 + m_3^2 = \frac{3}{2}. \tag{10}$$

We apply a basis transformation along with the parametric equation of a circle to derive the analytic solution. In this context, we define two unit vectors that lie on the plane: $\boldsymbol{v} = [-\frac{1}{\sqrt{2}}, \frac{1}{\sqrt{2}}, 0]^T$ and $\boldsymbol{u} = [\frac{1}{\sqrt{6}}, \frac{1}{\sqrt{6}}, -\frac{2}{\sqrt{6}}]^T$. These vectors form an orthonormal basis for the plane. Using this basis, we can re-express any encoded values on the plane in terms of these vectors:

$$\boldsymbol{m} = r(\boldsymbol{u}\cos\theta + \boldsymbol{v}\sin\theta). \tag{11}$$

Here, r represents the polar diameter. By combining Eqn. (11) and Eqn. (10), we obtain $r^2 = \frac{3}{2}$. Therefore, the analytic solution for the encoded values on the plane can be expressed as:

$$\begin{bmatrix} m_1 \\ m_2 \\ m_3 \end{bmatrix} = \begin{bmatrix} \frac{1}{2} & -\frac{\sqrt{3}}{2} \\ \frac{1}{2} & \frac{\sqrt{3}}{2} \\ -1 & 0 \end{bmatrix} \begin{bmatrix} \cos\theta \\ \sin\theta \end{bmatrix} = \begin{bmatrix} \cos(\theta + \frac{2\pi}{3}) \\ \cos(\theta + \frac{4\pi}{3}) \\ \cos(\theta + \frac{6\pi}{3}) \end{bmatrix}. \tag{12}$$

Eqn. (12) aligns with Eqn. (1) proposed in PSC, allowing PSC to be interpreted from a unified perspective of dimensional mapping.

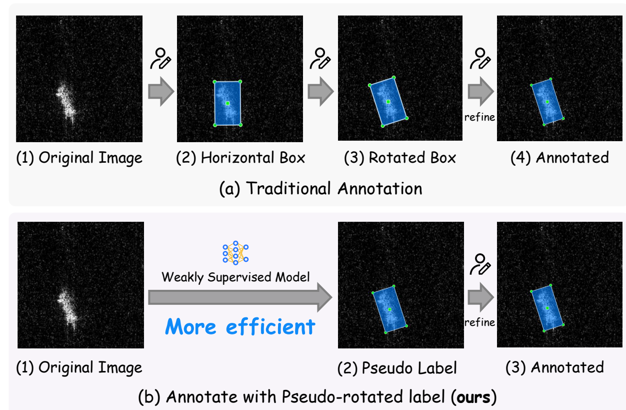

Figure 6. A comparison between the traditional annotation method and our approach, which uses pseudo-rotated labels from a weakly supervised model. It demonstrates our method simplifies and improves the efficiency of the annotation process.

B. Detail in Dataset Annotation

Fig. 6 illustrates a comparison between our annotation method and the traditional annotation method. Notably, the general practice for rotated annotation involves using a rectangular box, requiring the adjustment to begin with a horizontal rectangle. In the traditional method, the process begins by roughly determining a horizontal bounding box based on the object's position, followed by rotating the box to align with the object's orientation and finally fine-tuning its position. In contrast, our method employs a weakly supervised model to generate pseudo-rotated labels with high accuracy, requiring only minimal manual fine-tuning, which greatly enhances annotation efficiency.

Additionally, the angle adjustment step can be entirely skipped when the angle predictions are sufficiently accurate. Thus, this paper aims to improve the weakly supervised model's accuracy in angle prediction. To minimize the impact of pseudo-labels on manual labeling, traditional methods are used to label both the validation and test sets to avoid evaluation bias.

C. Additional Experiment Results

C.1. Multi-dimensional Mapping

To simplify optimization and computation, we focus on two-dimensional mapping and three-dimensional mapping of UCR in this study. For higher-dimensional mappings, encoded values must satisfy more additional constraints. Using four-dimensional mapping and five-dimensional map-

Resolver	DM	AP_{50}	AP_{75}	mAP
PSC [58]	4	71.98	40.03	41.25
UCR (**ours**)	4	73.76	41.62	42.67
PSC [58]	5	72.33	38.69	39.89
UCR (**ours**)	5	73.85	42.86	42.98

Table 7. A comparison of previous methods with our UCR approach in higher-dimensional mappings. All experiments are based on H2RBox-v2 [60]. Our method achieves superior performance in higher-dimensional mapping scenarios.

r^2	RSAR			DOTA-v1.0 [45]		
	AP_{50}	AP_{75}	mAP	AP_{50}	AP_{75}	mAP
0.5	67.89	23.96	31.75	73.18	41.37	42.05
1.5	68.33	26.17	32.64	73.99	42.10	43.10
3.0	68.45	23.37	32.00	73.78	41.31	42.03

Table 8. Ablation experiment on different ranges of mapping in three-dimensional mapping. Constraining the mapping range to unit space yields better results.

ping as examples, we define the corresponding constraints and conduct experimental validation on the DOTA-v1.0 dataset.

For a four-dimensional mapping, each encoded value must satisfy the following conditions:

$$\begin{cases} \sum_{i=1}^{4} m_i^2 = 2 \\ m_1 + m_3 = 0 \\ m_2 + m_4 = 0 \end{cases} . \tag{13}$$

For a five-dimensional mapping, each encoded value must satisfy the following conditions:

$$\begin{cases} \sum_{i=1}^{5} m_i^2 = 2.5 \\ \sum_{i=1}^{5} m_i = 0 \\ \sum_{i=1}^{5} m_i^3 = 0 \end{cases} . \tag{14}$$

Table 7 presents the results of experiments on higher-dimensional mappings. The results indicate that our UCR achieves greater performance improvements than the previous resolvers in higher-dimensional scenarios. However, as the number of mapping dimensions increases, the constraints become more complex. Therefore, we primarily focus on two-dimensional and three-dimensional mappings.

C.2. The Range of Mapping

In Sec. 3.1, we mention that there are multiple ways in which one-dimensional values can be mapped to a circle in multi-dimensional space. To simplify, we restrict the mapping range to unit space (*i.e.*, each dimension has a value range of $[-1, 1]$) and present the formula for Eqn. (4). If this constraint of unit space is removed, we obtain a new mapping form (*i.e.*, $\sum_i^n m_i^2 = r^2$, where $r > 0$). To validate the influence of different mapping forms on the model, we utilize three-dimensional mapping as an example and present the experimental results in Table 8. The experimental results indicate that the model achieves optimal performance when $r^2 = 1.5$ (*i.e.*, unit space). A larger mapping range can lead to more dispersed encoding states, making optimization and prediction more challenging. Conversely, a smaller mapping range may cause reduced differences between encoding states, resulting in prediction biases. Overall, restricting the mapping to unit space provides a more generalized approach, resulting in better performance for angle prediction.

$m_{invalid}$	AP_{50}	AP_{75}	mAP
0	73.16	40.94	41.68
0.1	73.21	41.62	41.89
0.2	73.22	42.26	42.65
0.5	73.13	40.98	41.92
1.0	39.56	7.87	14.42

Table 9. Ablation experiments on different ranges of the invalid region conducted by two- dimensional mapping of UCR. Optimal results are achieved when the threshold is taken as 0.2.

Method	SH	AI	CA	TA	BR	HB
▼ *One-stage*						
RetinaNet [38]	73.6	73.5	73.6	22.4	49.6	53.4
R^3Det [52]	78.7	73.2	89.3	22.6	56.9	63.0
S^2ANet [6]	82.3	77.8	89.8	25.8	60.2	63.0
FCOS [23]	79.0	73.0	89.8	33.9	58.8	65.5
▼ *Two-stage*						
Faster RCNN [34]	78.3	76.8	89.5	30.8	54.7	49.0
O-RCNN [46]	79.4	75.3	89.7	29.7	56.2	58.5
ReDet [7]	79.0	78.1	89.5	25.6	55.0	61.1
RoI-Transformer [5]	85.9	76.5	90.1	27.5	57.4	64.4
▼ *DETR-based*						
Deformable DETR [71]	58.0	51.3	66.5	21.7	36.8	45.4
ARS-DETR [61]	76.9	70.2	80.4	29.1	51.2	59.1

Table 10. The detailed fully supervised performance in various detectors on RSAR. All results present AP_{50} for each category.

C.3. The Range of Invalid Region.

Table 9 illustrates the effect of various invalid region ranges on the performance of the weakly supervised model. The findings reveal that incorporating the invalid region enhances model learning; however, extensive invalid regions may lead to insufficient constraints for angle regression.

C.4. Detailed Results on Fully Supervised Model

Table 10 summarizes the performance of various fully supervised models on the RSAR dataset, detailing the results for each category. The performance is evaluated using the AP_{50} metric, with categories represented by their respective abbreviations: Ship (SH), Aircraft (AI), Car (CA), Tank (TA), Bridge (BR), and Harbor (HA).